

Properties of a Luttinger Liquid with Boundaries at Finite Temperature and Size

Ann E. Mattsson, Sebastian Eggert, and Henrik Johannesson

Institute of Theoretical Physics, Chalmers University of Technology and Goteborg University, S-412 96 Goteborg, Sweden

We use bosonization methods to calculate the exact finite-temperature single-electron Green's function of a spinful Luttinger liquid confined by open boundaries. The corresponding local spectral density is constructed and analyzed in detail. The interplay between boundary, finite-size and thermal effects are shown to dramatically influence the low-energy properties of the system. In particular, the well-known zero-temperature critical behavior in the bulk always crosses over to a boundary dominated regime in the vicinity of the Fermi level. Thermal fluctuations cause an enhanced depletion of spectral weight for small energies ω , with the spectral density scaling as ω^2 for ω much less than the temperature. Consequences for photoemission experiments are discussed.

71.10.Pm, 71.27.+a

I. INTRODUCTION

In the last decade there has been an enormous interest in metallic phases of matter which are not Fermi liquids. A paradigm for these is the Luttinger liquid, describing the low-energy, long-wavelength limit of gapless electron systems in one dimension (1D)^{1,2}. The Luttinger liquid satisfies Luttinger's theorem, but the interaction wipes out the quasi-particle pole of the electron propagator, with the disjoint Fermi surface (consisting of two Fermi "points" k_F) supporting only collective charge- and spin density excitations. These excitations are dynamically independent, effectively leading to a spatial separation of the charge and spin of an electron added to the system. As a result, spectral properties and dynamical correlations are quite different from those of a Fermi liquid³.

The generic low-energy properties of a gapless interacting 1D electron system are well understood^{1,3} in terms of universal power-laws of correlation functions and spectral functions. The behavior of such so-called Luttinger liquids is coded in the Tomonaga-Luttinger model⁴, much in the same way as the normal state of 3D interacting electrons is patterned on the free Fermi gas (Landau Fermi liquid theory). However, it is only in the last few years that laboratory technology has advanced to the point that the notion of a Luttinger liquid can be confronted with experiments. Indeed, the ability to manufacture true 1D quantum wires^{5,6}, as well as the development of high-precision spectroscopic techniques for probing quasi-1D materials⁷, have provided strong impetus for investigating Luttinger liquid physics in realistic contexts. Added motivation comes from the realization that the edge excitations of the fractional quantum Hall effect can be described in terms of a chiral Luttinger liquid⁸. Also, some of the "non-Fermi liquid scenarios" for the normal state properties of the cuprate superconductors draw heavily from Luttinger liquid theory, suggesting possible extensions to higher dimensions⁹.

Whereas Luttinger liquid theory has been successfully used to predict fractional quantum Hall edge state transport^{10,11,12}, its applicability to the more traditional realm of quasi-1D materials remains controversial. This class of materials contains organic conductors such as tetrathiafulvalene-tetracyanoquinodimethane (TTF-TCNQ) and the tetramethyltetraselenafulvalene (TM(TSF)₂X) Bechgaard salts with $X = \text{ClO}_4; \text{PF}_6$; etc. All available information suggests that the physics of these compounds is dominated by strong electron correlations and pronounced one-dimensionality^{3,13}. Yet, data from NMR¹⁴ and photoemission spectroscopy⁷ interpreted within a conventional Luttinger liquid framework seem to imply single-electron correlations governed by an exponent much larger than can be provided from any realistic lattice Hamiltonian (of which the Tomonaga-Luttinger model would be the effective low-energy continuum theory). This poses a major problem for the modeling of these materials, and its resolution remains a challenge for the theorist.

One of the basic quantities to consider in this context is the single-particle spectral density, as this is the object that determines the outcome of a photoemission experiment. Surprisingly, the full calculation of the spectral density of an ideal, infinite volume Luttinger liquid was only recently performed⁵, expanding upon earlier results by Suzumura¹⁶. In the present paper we go a step further and investigate the local, finite-temperature spectral density of a Luttinger liquid confined by open boundaries (simulating a reflecting barrier or edge potential). As photoemission spectroscopy measurements are highly sensitive to boundary effects (with the photoelectrons traveling only a short distance, of the order of a few lattice spacings from the surface of the sample), it is crucial to incorporate an analysis of nontrivial boundary conditions. Also, spectroscopy on high-mobility quantum wires doped with artificial impurities

(antidots")¹⁷ may soon be within experimental reach, adding yet another reason to study this problem: at sufficiently low temperatures a potential scatterer is expected to act essentially as a reflecting barrier¹⁰.

In the present paper we calculate the exact finite-temperature single-electron Green's function and the associated local spectral density of a confined spinful Luttinger liquid. The combined effects of boundaries and finite volume will be shown to strongly modify the well-known bulk Luttinger liquid spectral density. In particular, the presence of boundaries causes a novel scaling behavior for energies close to the Fermi level, which produce a depletion of spectral weight significantly larger than that for a bulk system, as we have reported for a semi-infinite system at zero temperature before¹⁸. In addition, thermal fluctuations deplete the levels further and give rise to a universal¹² scaling of the spectral density for sufficiently small frequencies!, which is analogous to the temperature effects in "bulk" systems¹⁹. Particular attention is given to the nontrivial zero mode contribution to the correlation function from fluctuations in the spin and charge quantum numbers, which turn out to violate the spin-charge separation (i.e. the partition function cannot be split into separate spin and charge factors). Interestingly, the confined system is sensitive to the ratio between the effective velocities for the collective charge- and spin excitations (which in turn depend on the effective electron-electron coupling): As the velocity ratio locks into a rational value the spectrum separates into distinct peaks of equal spacing. The spacing between the peaks becomes dense for irrational values of the velocity ratios, leading to a quasi-continuous spectrum for large!. This hints at a resonant interference between standing waves of charge and spin for special values of the electron-electron coupling.

The paper is organized as follows: In the next section we introduce an extended version of the Tomonaga-Luttinger model and review its bosonization in the presence of open boundaries. In Sec. III the full finite-temperature Green's function in a bounded domain is derived, and the resulting local spectral density is extracted and analyzed in Sec. IV. Section V contains a brief discussion of possible consequences for photoemission experiments, as well as some concluding remarks.

II. 1D ELECTRONS IN THE PRESENCE OF OPEN BOUNDARIES: BOSONIZATION

As our model we take an extension of the Tomonaga-Luttinger Hamiltonian⁴, which describes spinful Fermions in one-dimension with a (repulsive) local interaction. All electron-electron interactions must conserve spin and charge, so that we use the most general gapless Hamiltonian density that is invariant under the corresponding SU(2) and U(1) symmetries,

$$\begin{aligned}
 H = v_F & \int_{L,R} \psi^\dagger \left(i \frac{d}{dx} \right) \psi + \int_{L,R} \psi^\dagger \left(i \frac{d}{dx} \right) \psi; \\
 & + g_{2?} \int_{L,R} \psi_L^\dagger \psi_R + g_{2k} \int_{L,R} \psi_L \psi_R + g_{4?} (\int_{L,R} \psi_L^\dagger \psi_L + \int_{L,R} \psi_R^\dagger \psi_R) + g_{4k} (\int_{L,R} \psi_L \psi_L + \int_{L,R} \psi_R \psi_R) \\
 & + g_{1?} \int_{L,R} \psi_L^\dagger \psi_R; \int_{L,R} \psi_R^\dagger \psi_L; ;
 \end{aligned} \tag{1}$$

where we have used the traditional "g-ology" scheme to index the couplings²⁰. The chiral Fermion currents are defined as $J_{L=R} = \int_{L=R} \psi^\dagger \psi$; $J_{L=R}$; $J_{L=R}$; and $J_{L=R}$; $J_{L=R}$; (x) are the left/right moving components of the electron field $\psi(x)$ expanded about the Fermi points k_F ,

$$\psi(x) = e^{ik_F x} \psi_{L;}(x) + e^{ik_F x} \psi_{R;}(x); \tag{2}$$

This expansion is valid as long as the lattice spacing is much smaller than all length scales we want to consider. Therefore, the energy range around the Fermi-surface is limited to a region where a linear approximation of the spectrum is justified. This is often conveniently illustrated by a cut-off parameter, but more accurately one should take higher order operators in the Hamiltonian into account which result in corrections to the linear spectrum which are of higher orders in $k - k_F$. These perturbations have non-universal coefficients which depend on the detailed interactions of the underlying lattice Hamiltonian. The appropriate value of the cut-off parameter (i.e. the range of validity) is then determined by the momentum scale at which those corrections become so large that the perturbation series no longer converges. Generically we can only roughly estimate the range of validity to be about one order of magnitude less than the band-width.

The first term in Eq. (1) is that of free relativistic fermions, while g_2 and g_4 describe forward electron-electron scattering. We have also explicitly included a backward scattering term $g_{1?}$. The coupling constants depend on the microscopic parameters of the underlying lattice model and v_F is the Fermi velocity. Normal ordering is carried out w.r.t. the filled Dirac sea, and we sum over repeated spin indices.

Eq. (1) defines a "standard model" for low-energy electrons in a 1D metallic phase, and is easily derived from the Hubbard Hamiltonian

$$H_H = \sum_i U c_{i+1}^\dagger c_i + U \sum_i n_i n_{i+1}; \quad U > 0; \quad (3)$$

In the weak coupling limit $U \ll t$, we can treat U as a perturbation, and the tight-binding band $\epsilon(k) = -2t \cos(ka)$ may be linearized around the Fermi points $k_F = \pm \pi/2a$, n_e being the electron density and a the lattice spacing. The electron operators are replaced by the chiral fields $\psi_{L=R}$ in the continuum limit

$$c_{i\pm} = \frac{1}{\sqrt{a}} \int dx e^{ik_F x} \psi_{L=R}(x); \quad (4)$$

As a result, the Hubbard model gets mapped onto the Hamiltonian density in Eq. (1) with coupling constants $g_{1?} = g_{2?} = 2g_{4?} = U/a$ and $g_{2k} = g_{4k} = 0$. The Umklapp term $\sum_i c_{i+2}^\dagger c_i + \text{h.c.}$ is also generated, but does not contribute away from half-filling ($n_e \in \mathbb{Z}$; $k_F \in \pi/2a$) due to rapid phase oscillations. For this case we are left with the theory in (1), with $v_F = 2at \sin(k_F a)$. It is important to emphasize that the Hamiltonian in (1) faithfully represents the low-energy sector of the Hubbard model also for strong on-site repulsion U^{21} . However, when U is not small, the procedure above fails to identify the proper values of the model parameters, and instead these have to be inferred from the exact Bethe Ansatz solution of the Hubbard model^{21;22}.

The Hamiltonian (1) is conveniently bosonized²³ by introducing charge and spin currents and the corresponding bosons ϕ_c and ϕ_s with conjugate momenta π_c and π_s , respectively

$$J_L^{c=s} = \frac{1}{2} J_L^{\#} = \frac{1}{4} \partial_x \phi_{c=s} + \pi_{c=s}; \quad (5a)$$

$$J_R^{c=s} = \frac{1}{2} J_R^{\#} = \frac{1}{4} \partial_x \phi_{c=s} - \pi_{c=s}; \quad (5b)$$

The resulting theory describes separate spin and charge excitations moving with velocities (to lowest order in the coupling constants)

$$v_c = v_F + \frac{g_{4k}}{2} + \frac{g_{4?}}{2}, \quad v_s = v_F + \frac{g_{4k}}{2} - \frac{g_{4?}}{2}; \quad (6)$$

where $v_c > v_s$ for repulsive interactions $g_{4?} > 0$. The Hamiltonian becomes

$$H = \sum_{s;c} \int dx \frac{v}{2} (\partial_x \phi_{s;c})^2 + \frac{g}{4} (\partial_x \phi_{s;c})^2 + g_{1?} \cos \frac{2\phi_s}{a}; \quad (7)$$

where $g_c = g_{2k} + g_{2?}$ and $g_s = g_{2k} - g_{2?}$. The charge interaction g_c can be absorbed into the free Hamiltonian by a simple rescaling of the charge boson, but the spin interactions g_s and $g_{1?}$ obey Kosterlitz-Thouless renormalization group equations²⁴ with flow lines along hyperbolas $g_s^2 - g_{1?}^2 = \text{const.}$ (to lowest order). For $g_s > g_{1?}$ the spin sector develops a gap in the low energy, long wavelength limit, but for $g_s < g_{1?}$ the system flows to a stable fixed point $g_s = g_{1?}$; $g_{1?} = 0$. For $g_s = g_{1?}$ the interaction corresponds to one single marginally irrelevant operator, so that $g_s = g_{1?} = 0$. If the flow to a stable fixed point occurs, we can rescale the bosons by a canonical transformation to obtain a free theory ($g_{1?} = s;c$)

$$\phi_{s;c} = K_s \phi_{s;c}'; \quad \pi_{s;c} = \frac{1}{K_s} \pi_{s;c}'; \quad (8)$$

where to first order in the coupling constants

$$K_s^2 = 1 - \frac{g_{1?}}{g_s}; \quad K_c^2 = 1 - \frac{g_{1?}}{g_c}; \quad (9)$$

This yields the Hamiltonian

$$H = \sum_{s;c} \int dx \frac{v}{2} (\partial_x \phi_{s;c}')^2 + \dots \quad (10)$$

where $v = (v + \frac{g_{1?}}{2})K^2$, i.e. $v = v$ to first order in the coupling constants so we will omit the bar in the following.

The chiral components of the electron field can now be expressed in terms of free boson fields and their duals by using Eq. (5) and the formula²⁵

$$\psi_{L=R}(x) = \frac{1}{\sqrt{2}} \exp \left[\pm i \int dx J_{L=R}(x) \right]; \quad (11)$$

where ψ obeys the anticommutation relation $\{\psi, \psi^\dagger\} = 0$, with $\psi^2 = 1$. The presence of ψ in (11) guarantees that operators with different spin obey anticommutation relations.

Using the duality relation $\psi_t = \psi_x^\sim$, we thus obtain, using Eqs. (5) and (8)

$$\psi_{L=R}; (\mathbf{x}) / \psi_{=c;s} = \exp i \int_{-r}^r K(\mathbf{x}) K^{-1\sim}(\mathbf{x}) ; \quad (12)$$

with $\psi = 1$ unless $\psi = s$ and $\psi = \#$ when it is equal to $\psi = 1$. Note that we have obtained the bosonization formula (12) with no assumption about boundary conditions.

We now apply the formalism above to a system of length L with open boundary conditions and thus require the electron field $\psi(\mathbf{x})$ to vanish at $x = 0$ and at $x = L$. From Eq. (2) we see that this implies

$$\psi_L; (0;t) = \psi_R; (0;t) \quad (13a)$$

$$\psi_L; (L;t) = e^{i2k_F L} \psi_R; (L;t) : \quad (13b)$$

Considering Eq. (12) this gives us fixed boundary conditions on the boson fields, which in turn determine the mode expansion.

To calculate the mode expansion for the boson we find it most convenient to consider the classical Euler-Lagrange equation with fixed boundary conditions at $x = 0;L$

$$\psi(0;t) = C_0; \quad \psi(L;t) = C_L; \quad (14)$$

and then performing a canonical quantization. We therefore consider the classical Lagrangian density corresponding to the Hamiltonian (10)

$$L = \sum_{s;c} \frac{v}{2} (\psi_{v,t})^2 - (\psi_x)^2 \quad (15)$$

where $\psi_{v,t} = \frac{1}{v} \psi_t$. The resulting Euler-Lagrange equations can be expressed in terms of $\psi = \psi_x - \psi_{v,t}$,

$$(\psi_{v,t}^2 - \psi_x^2) = \psi_+ \psi_- = 0; \quad (16)$$

and it follows that the two solutions can be written in terms of left- and right moving bosons, $\psi_{;L}(x + vt)$ and $\psi_{;R}(x - vt)$. We use the combination $\psi(x;t) = \psi_{;L}(x + vt) + \psi_{;R}(x - vt)$ and its dual field $\psi^\sim(x;t) = \psi_{;L}(x + vt) - \psi_{;R}(x - vt)$, related by

$$\psi_x = \psi_{v,t}^\sim; \quad \psi_x^\sim = \psi_{v,t} : \quad (17)$$

The classical solution with the boundary condition (14) is obtained in a straightforward way, and after canonically quantizing we find the mode expansion for the quantum fields according to the boundary condition (13)

$$\psi(x;t) = \psi_{;0} + \hat{Q} \frac{x}{L} + \sum_{n=1}^{\infty} \frac{1}{n} \sin \frac{n x}{L} e^{i \frac{n v t}{L}} a_n + h.c. ; \quad (18a)$$

$$\psi^\sim(x;t) = \psi_{;0} + \hat{Q} \frac{v t}{L} + \sum_{n=1}^{\infty} \frac{1}{n} \cos \frac{n x}{L} e^{i \frac{n v t}{L}} a_n + h.c. : \quad (18b)$$

The non-zero commutation relations among the mode operators are $[a_n; a_n^\dagger] = 1$ and $[\psi_{;0}; \hat{Q}] = i$, while $\psi_{;0}$ are c-numbers. This result (18) obtained from the classical solution automatically contains the correct zero modes, in particular the total charge and spin operators \hat{Q} , which were first postulated by Haldane for a periodic system¹. The resulting energy spectrum from Eq. (10) is

$$H = \sum_{s;c} \frac{v}{2L} \hat{Q}^2 + \sum_{n=1}^{\infty} \frac{v n}{L} a_n^\dagger a_n : \quad (19)$$

From Eqs. (18) we can read off the mode expansions for left-moving bosons

$$\begin{aligned}
\psi_L(x;t) &= \frac{1}{2} \left(\psi(x;t) + \tilde{\psi}(x;t) \right) \\
&= \frac{1}{2} \left(\psi_{;0} + \tilde{\psi}_{;0} + \hat{Q} \frac{x+vt}{2L} + \sum_{n=1}^{\infty} \frac{1}{n} e^{i \frac{n(x+vt)}{L}} a_n + \text{h.c.} \right)
\end{aligned} \quad (20)$$

The right-moving boson field can be related to the left-moving one by

$$\psi_R(x;t) = \frac{1}{2} \left(\psi(x;t) - \tilde{\psi}(x;t) \right) = \psi_L(-x;t) + \psi_{;0} \quad (21)$$

The boundary conditions (13) on the fermions provide us with the quantization condition for the eigenvalues of the operators \hat{Q} (using special commutation relations of ψ and $\tilde{\psi}$ at the boundary²⁶ that follow from the mode expansion (18))

$$K_c Q_c = \frac{r}{2} \left(n + 1 + \frac{2k_F L}{r} \right) ; \quad (22a)$$

$$K_s Q_s = \frac{r}{2} m ; \quad (22b)$$

where m and n are either both odd or both even integers. Therefore, the quantum numbers for the total spin m and the total charge n are not independent, which is to be expected because we can only insert and remove real electrons, i.e. we cannot change the total charge and the total magnetization independently. In this sense these degrees of freedom do not obey spin-charge separation and the partition function does not factorize. It is interesting to note the formal similarity to a spinless periodic system, which is also described by two channels (left and right moving) and where a similar condition holds for the total current and charge quantum numbers⁴. As we will see later, the zero modes indeed give a contribution to the Green's function which does not factorize, while all dynamical degrees of freedom in Eq. (19) remain spin-charge separated.

The constants $c_{;0} = \frac{r}{2} K_c^{-1}$ and $s_{;0} = 0$ are also determined by the boundary condition (modulo the intrinsic periodicity of the boson $2\pi K^{-1}$). Hence, we obtain from Eqs. (12) and (21)

$$\psi_R(x;t) = \psi_L(-x;t) \quad (23)$$

which allows us to write the full theory in terms of left-movers only. This concludes our analysis of bosonization in the presence of open boundaries. For an alternative approach – exploiting the path integral formulation – see Ref. 27.

III. GREEN'S FUNCTIONS

Using the formalism above, the exact single electron Green's function for a confined Luttinger liquid with open boundaries can now be calculated. With the decomposition in Eq. (2) and using Eq. (23), we have

$$\begin{aligned}
G^y(x;t) G^y(y;0) &= e^{ik_F(x-y)} G(x;y;t) + e^{-ik_F(x-y)} G(-x;y;t) \\
&= e^{ik_F(x+y)} G(x;-y;t) + e^{ik_F(x+y)} G(-x;y;t);
\end{aligned} \quad (24)$$

where the chiral Green's function $G(x;y;t) = G_{L;}(x;t) G_{L;}(y;0)$ is derived in Appendix A. The result is a product of the spin and charge contributions $F_{s;c}$ and a factor H from the zero modes

$$\begin{aligned}
G(x;y;t) / H(x;y;t) &= F_{c;s}^y \left(F(vt+x-y) \right)^{\frac{(K+K^{-1})^2}{8}} \left(F(vt-x+y) \right)^{\frac{(K-K^{-1})^2}{8}} \\
&= \frac{F(2x) F(2y)}{F(vt+x+y) F(vt-x-y)} e^{\frac{K^2 - K^{-2}}{8}} ;
\end{aligned} \quad (25)$$

The contribution H from the zero modes is given by (see Appendix A)

$$H(x;y;t) = \frac{\#_2(u_c + c k_F L j_c) \#_3(u_s j_s) + \#_3(u_c + c k_F L j_c) \#_2(u_s j_s)}{\#_2(-c k_F L j_c) \#_3(0 j_s) + \#_3(c k_F L j_c) \#_2(0 j_s)} e^{i2u_c \frac{k_F L}{2}} \quad (26)$$

where the Theta functions, $\theta_k(u_j)$, are defined in sections 8.18-8.19 in²⁸ and

$$u = \frac{v}{2} \frac{K^2 t + x - y}{L} = \frac{v}{K^2 L} : \quad (27)$$

The expression for H does not contain any poles, but may still influence the spectral properties significantly in mesoscopic systems^{29;30}. It is also interesting to note that the contribution from the zero modes cannot be written as a product of independent spin and charge contributions, which is expected since the quantum numbers n and m in Eq. (22) are not independent.

The factors F from the spin and charge bosonic modes can also be written in terms of the Theta functions (see sections 8.18-8.19 in²⁸)

$$F(z) = i \frac{2L}{z} \prod_{k=1}^2 \sin \frac{z}{2L} \left[1 + \frac{\sin \frac{z}{2L}}{\sinh k \frac{v}{2L}} \right] = \frac{\theta_1 \left(\frac{z}{2L} \middle| \frac{v}{2L} \right)}{\theta_1 \left(i \frac{z}{2L} \middle| \frac{v}{2L} \right)} : \quad (28)$$

Here x and y denote the distance from the left boundary ($x = 0$) and the argument z carries an implicit cut-off $z \ll i$. The parameters v and K are defined in (6) and (9) respectively.

We can immediately verify that the full Green's function is anti-periodic under translation by the inverse temperature $t \rightarrow t + i$ as it should be. It is also interesting to note that the factor from the zero modes is periodic under the change of the Fermi-level k_F by π/L , which results in periodic oscillations of the spectral properties of the system as the chemical potential is changed. This is a manifestation of Coulomb blockade oscillations, i.e. resonances can be observed if the system is of "mesoscopic" size³⁰. It is important to emphasize that the zero mode contribution H in Eq. (26) is obtained by using a grand canonical ensemble when taking the averages, thus allowing for fluctuations in the magnetization m and in the particle number n . By fixing these quantum numbers (i.e. using an idealized "closed" system) or by letting the system size tend to infinity, the zero mode contribution collapses to a constant phase. This provides a vivid example of how different statistical ensembles may lead to different results on mesoscopic scales and downwards, where quantum coherence effects become important³¹.

We see in Eq. (25) that we recover the universal power-laws, which give the expected branch cuts in the Green's function³. In addition, we get a contribution from the boundary, which is entirely contained in the last factor of Eq. (25) and gives an additional analytic structure. This factor does not contribute in non-interacting systems ($K_c = K_s = 1$), so that in this case the presence of the boundary is seen only by the addition of the two last "Friedel" terms in Eq. (24) compared to the bulk case. In contrast, with interaction ($K_s; K_c < 1$), the boundary influences also the chiral Green's function. This is expected, since only with interactions can effects from electron scattering on the boundary propagate to other parts of the system, thus influencing also the chiral pieces of the full Green's function.

The zero-temperature limit $T \rightarrow 0$ is readily obtained by letting $\beta \rightarrow 1$ in Eqs. (26) and (28)

$$G(x;y;t) / e^{i(2n_0 - 1)u_c} = \prod_{c;s} \frac{2L}{\sin \frac{(v t + x - y)}{2L}} \frac{(K_c + K_s - 1)^2}{8} \frac{2L}{\sin \frac{(v t - x + y)}{2L}} \frac{(K_c - K_s - 1)^2}{8} \frac{\sin \frac{x}{L} \sin \frac{y}{L}}{\sin \frac{(x+y+vt)}{2L} \sin \frac{(x-y-vt)}{2L}} \frac{(K_c^2 - K_s^2)}{8} \quad (29)$$

where $n_0 = (k_F L \bmod 1)$ effectively measures the difference between the Fermi-vector and the highest occupied level (which are not necessarily the same in a system with discrete energy levels). The phase $e^{i(2n_0 - 1)u_c}$ comes from the zero modes and does influence the time correlations. For special values of n_0 this phase may have a different dependence on u . When this phase is neglected, Eq. (29) agrees with the results in Ref. 32, obtained via bosonization according to the "Haldane prescription"¹. It is also in agreement with results¹⁸, obtained by conformally mapping the semi-infinite complex plane onto a finite strip.

Using the Poisson summation formula, we can obtain the limits of the Theta functions $\theta_1(z|\tau) \xrightarrow{\tau \rightarrow 2} e^{-z^2} = e^{-4} \sinh z$ and $\theta_2(z|\tau) \xrightarrow{\tau \rightarrow 2} e^{-z^2} = 1$ as $\beta \rightarrow 0$. Hence, by letting $L \rightarrow 1$ in Eqs. (26) and (28), we obtain the finite temperature chiral Green's function of a semi-infinite system with open boundary

$$G(x;y;t) / \prod_{c;s} \frac{v}{\sinh \frac{(v t + x - y)}{v}} \frac{(K_c + K_s - 1)^2}{8} \frac{v}{\sinh \frac{(v t - x + y)}{v}} \frac{(K_c - K_s - 1)^2}{8}$$

$$\frac{\sinh \frac{2x}{v} \sinh \frac{2y}{v}}{\sinh \frac{(x+y+v t)}{v} \sinh \frac{(x+y-v t)}{v}} \frac{K_c^2 K_s^2}{8} : \quad (30)$$

Finally, the $T \rightarrow 0$ limit for a semi-infinite system is obtained by letting $v \rightarrow 1$ in Eq. (30) (or $L \rightarrow 1$ in Eq. (29)):

$$G(x;y;t) / \frac{4xy}{[(x+y)^2 - v^2 t^2]} \frac{K_c^2 K_s^2}{8} : \quad (31)$$

We note that in the limit $xy \gg (x-y)^2 \gg v^2 t^2$ the last factor in equation (31) goes to unity and we recover the known zero-temperature bulk correlation function³ (as we also do in the non-interacting case $K_c = K_s = 1$). In the limit of equal time, $t = 0$, this gives the asymptotic correlator

$$G(x;y;t=0) / \frac{1}{(x-y)^2} \quad (32)$$

with the equal-time bulk exponent $\nu = (K_c^2 + K_s^2 + K_c^2 + K_s^2) = 8$. In contrast, when one of the points is close to the boundary compared to the relative distance $x \sim y$ one finds

$$G(x;y;t=0) / \frac{1}{(x-y)^{\nu_?}} ; \quad (33)$$

with $\nu_? = (3K_c^2 + 3K_s^2 + K_c^2 + K_s^2) = 16$. This is to be compared to the asymptotic long-time behavior of the autocorrelation function in the limit $t \gg x, y$, which behaves as

$$G(x;x;t) / \frac{1}{t^{2\nu_k}} \quad (34)$$

with $\nu_k = (K_c^2 + K_s^2) = 4$. As expected from scale invariance, we thus recover the scaling law $\nu_? = (\nu + \nu_k) = 2$. It may be worth pointing out that the dynamic ($t \neq 0$) asymptotic large distance correlator in Eq. (33) is not governed by the single exponent $\nu_?$, as one may naively have expected from the analogy with classical critical phenomena³³. Instead it remains a product of separate charge- and spin correlators with exponents $(3K_c^2 + K_c^2) = 16$ and $(3K_s^2 + K_s^2) = 16$, respectively. This is not in conflict with scale invariance since the theory is built out of two distinct sectors, each with its own effective velocity. More importantly, the behavior in Eq. (34) reveals that the asymptotic low-energy behavior of a Luttinger liquid with an open boundary belongs to a different universality class than that of the bulk theory. We shall elaborate on this in the next section when we discuss the local density of states.

IV. LOCAL SPECTRAL DENSITY

To understand the physical implications of the boundary correlations we study the local spectral density $N(\omega; r)$, given in terms of the single electron Green's function in (24)

$$N(\omega; r) = \frac{1}{2} \int_{-1}^1 e^{i\omega t} \langle \psi(r;0) \psi(r;t) \rangle dt; \quad (35)$$

where ω is measured relative to the Fermi energy and r is the distance from the boundary.

At $T = 0$ and without the boundary, the integral in (35) can be done exactly¹⁵ and one finds that the spectral density scales at the Fermi level as $N(\omega) / \omega^{-\nu_{\text{bulk}}}$, where the exponent in the bulk is given by

$$\nu_{\text{bulk}} = (K_c^2 + K_c^2 + K_s^2 + K_s^2) = 4 - 1; \quad (36)$$

However, the boundary clearly influences this scaling behavior, and by inspection of Eq. (31) for a semi-infinite system at $T = 0$, simple power counting reveals that there must be a crossover to a boundary dominated regime for $r \ll v_c, v_s$ with a novel exponent

$$\nu_{\text{bound}} = (K_c^2 + K_s^2) = 2 - 1; \quad (37)$$

Interestingly, the boundary exponent ν_{bound} therefore always dominates for sufficiently small r . It is also interesting to note that the last two terms in equation (24) make a contribution which oscillates at twice the Fermi wave-vector and

drops off with the distance from the boundary proportional to $e^{-2k_F r} (K_c^2 + K_s^2)^{-2}$. This contribution is reminiscent of a Friedel oscillation, although it can probably not be observed directly, since experimental measurements of the density of states (in particular photoemission) effectively averages over several lattice sites. We therefore ignore those "Friedel" terms in the following calculations and make the replacement

$$G(x; y; t) \rightarrow G(x; x; t) + G(x; y; t) + G(y; x; t) + G(y; y; t); \quad (38)$$

in Eq. (35). Using our exact results for $G(x; y; t)$ in the previous section allows us to fully explore the physically relevant piece of the local spectral density.

A. The zero temperature and infinite length limit

For $T \rightarrow 0$ and a semi-infinite system, $L \rightarrow 1$, it is readily derived from (31), (35) and (38) that

$$N(\omega; T=0; r) = \frac{2}{v_c} v_c^{a_c} v_s^{a_s} \int_0^1 dt \cos(\omega t) \cos\left(t \left[1 - \frac{v_c t}{2r}\right]^{b_c=2} \left[1 - \frac{v_s t}{2r}\right]^{b_s=2}\right) \quad (39)$$

where

$$\omega(t) = \begin{cases} \frac{8}{2} (a_s + a_c) & 0 < t < \frac{2r}{v_c} \\ \frac{8}{2} (a_s + a_c + b_c) & \frac{2r}{v_c} < t < \frac{2r}{v_s} \\ \frac{8}{2} (a_s + a_c + b_s + b_c) & \frac{2r}{v_s} < t < 1 \end{cases} \quad (40)$$

and

$$a = \frac{K_c^2 + K_s^2}{4}; \quad b = \frac{K_c^2 - K_s^2}{4}; \quad (41)$$

To cure the original divergences in (39) we have subtracted an infinite constant by renormalizing the static spectral density to zero for any given r , i.e. $N(\omega=0; T=0; r) = 0$.

Let us study the two limiting cases $r \rightarrow 0$ (boundary regime, with the short-distance cutoff) and $r \rightarrow 1$ (bulk regime). Both limits are easily obtained from Eq. (39) by using the integral (3.823 in²⁸)

$$\int_0^1 dx (\cos x - 1) x^{-k} = \frac{1}{(k-2) \cos \frac{\pi}{2} k} \quad 1 < k < 3; \quad (42)$$

with $\Gamma(k)$ the Gamma function. This gives

$$N(\omega) = \begin{cases} \frac{8}{(1 + \text{bulk})} \Gamma(\text{bulk}) & r \rightarrow 1 \\ \frac{8}{(1 + \text{bound})} \Gamma(\text{bound}) & r \rightarrow 0 \end{cases} \quad (43)$$

where $\text{bulk} = a_s + a_c - 1$ and $\text{bound} = a_s + a_c + b_s + b_c - 1$. In the bulk limit $r \rightarrow 1$ this result is in full agreement with previous calculations^{15;16}, but in the boundary limit $r \rightarrow 0$ we observe completely different exponents. By substituting ωt by x in the integral in Eq. (39) we see that apart from a prefactor measuring the distance to the boundary, the spectral density depends only on the scaling variable $r t$. This implies that the condition for boundary behavior is $\frac{r t}{v_c} \ll 1$, i.e. regardless of the value of r there will always be a region in ω around the Fermi-energy where the spectral density is determined by the boundary exponent bound . Actually, the scaling behavior of the spectral density splits into three distinct regions in ω where different exponents govern the leading scaling.

As an example, let us choose parameters adapted to a description of the large- U Hubbard chain away from half-filling (cf. Sec. II and Ref. 3). In this case the SU(2)-invariance forces $K_s = 1$, and it is known from Bethe ansatz calculations that $K_c^2 \rightarrow 1=2$ when $U \rightarrow 1$ ^{21;22}. Therefore, the spin channel is not affected by the boundary (since $b_s = 0$), and the local spectral density $N(\omega; r)$ in Eq. (39) splits into two asymptotic sectors only: The boundary regime for $\omega < \frac{v_c}{r}$ and the bulk regime for $\omega > \frac{v_c}{r}$. From these numbers, the well known result $N(\omega) \sim |\omega|^{-8}$ follows immediately for the bulk regime, as can be seen from Eq. (43). In the presence of the boundary, however, we cross over to the boundary exponent $\text{bound} = 1=2$ for $\omega < v_c/r$. The results in Fig. (1) clearly show the crossover from boundary behavior for $r t = v_c < 1$ with exponent $\text{bound} = 1=2$ to bulk behavior for $r t = v_c > 1$ with exponent $\text{bulk} = 1=8$ (the corresponding power-laws are superimposed). In the figure, the distance from the boundary, r , is held constant, thus setting the scale. The observed oscillations in Fig. (1) are an intriguing secondary effect, which vanish asymptotically as $\sin(2! r = v_c) (r t)^{b_c=2-1}$. It is important to emphasize that they are not due to the "Friedel" terms in equation (24) which have been neglected. Instead, they originate from the integrable singularity of the integrand in Eq. (39) at $t = \frac{2r}{v_c}$, which is only present in the boundary case.

B. The finite temperature and infinite length limit

We now consider the effect of finite temperatures on a semi-infinite system with a boundary. In general, by turning on temperature one induces a different behavior for small ω : Both in bulk and boundary regimes (defined as above) the spectral density crosses over to ω^2 scaling when $\omega < 2T$. This is due to thermal fluctuations which produce exponential damping of the density correlations for unequal times. The formal expression for $N(\omega; r)$ for this case, with $\beta = 1/k_B T$ and $k_B = 1$ is given by

$$N(\omega; r) = \frac{2}{2} v_c^{a_c} v_s^{a_s} \int_0^{\beta} dt \cos(\omega t)^4 \cos^2 t \frac{\sinh -t}{-} \frac{\sinh \frac{\omega}{v_c} (2r + v_c t) \sinh \frac{\omega}{v_c} (2r - v_c t)}{\sinh^2 \frac{2r}{v_c}} \quad (44)$$

$$\frac{\sinh \frac{\omega}{v_s} (2r + v_s t) \sinh \frac{\omega}{v_s} (2r - v_s t)}{\sinh^2 \frac{2r}{v_s}} \quad \frac{t}{1} \frac{v_c t}{2r} \quad \frac{v_s t}{2r} \quad 5;$$

where $\langle t \rangle$ is given in Eq. (40). We have subtracted the same infinite constant as in Eq. (39), thereby, as before, renormalizing the zero-temperature static spectral density to zero for any given r , i.e. $N(\omega = 0; T = 0; r) = 0$.

Substituting ωt by x in the integration of Eq. (44) as above reveals that $N(\omega; r)$ can be expressed as a function of two scaling variables $r\omega$ and ω (up to the same r -dependent prefactor as for zero temperature). By inspection we recover the $T = 0$ result when $\frac{\omega}{2} \gg 1$, but for small ω a new behavior sets in. Independently of whether we are in the boundary or bulk region, $N(\omega; r) \sim N(0; r)$ will be proportional to ω^2 for small ω !

$$N(\omega; r) \sim N(0; r) / \int_0^{\beta} dt (\cos \omega t - 1) \sinh -t$$

$$= 2 \int_0^{\beta} dx (\sinh x)^k \sin^2 \frac{\omega}{2} x \quad \frac{1}{2} - \int_0^{\beta} dx (\sinh x)^k x^2 \quad (45)$$

where the last integral converges if $0 < k < 3$ (in our case $k = n + 1$ where n is the boundary or bulk exponent). In conclusion, the spectral properties are unaffected for energies well above the temperature $\omega \gg 2T$, as expected. However, the spectral density will exhibit a ω^2 behavior for $\omega < 2T$ before the cross-over to the $T = 0$ behavior occurs, as can be seen in Fig. (2) where we again have considered the large- U Hubbard model away from half-filling. This is in complete agreement with the recent work by Nakamura and Suzumura¹⁹ where the analogous effect was reported for an infinite "bulk" system. Effectively, Fig. (2) contains all information about both the bulk and the boundary case, since we are free to adjust the distance from the boundary r to any value and this only changes the scale on which we measure the energies and temperatures. Therefore, we observe a cross-over from the quadratic behavior directly to bulk behavior if $\frac{\omega}{2} > 1$, while an intermediate boundary region can be observed for $\frac{\omega}{2} < 1$. As we can see in Fig. (2), the spectral density can look very flat around the Fermi-level in either case, and the sharp cusp which has been predicted for $T = 0$ may not at all be visible in experiments.

It is interesting to note that the boundary exponent also shows up in the temperature dependence of the static spectral density $N(\omega = 0; r)$. This is expected since the static density samples all times, with the asymptotic large-time behavior governed by the boundary exponent. As can be obtained from (44),

$$N(\omega = 0; r) = \frac{2}{2} (v_c^{a_c} v_s^{a_s})^{a_s + a_c - 1} \frac{\text{bound} (\frac{2r}{v_c})^{b_c} (\frac{2r}{v_s})^{b_s} C(\text{bound} + 1)}{\text{bulk} C(\text{bulk} + 1)} \quad \frac{2r}{v_s} \quad 1$$

$$\frac{2r}{v_c} \quad 1 \quad (46)$$

where

$$C(k) = \cos \frac{k}{2} \int_0^{\beta} dx \sinh^k x \quad x^k \quad (47)$$

which is convergent for $1 < k < 3$. With parameters again chosen to describe the large- U Hubbard chain (away from half-filling), the boundary dominated regime opens up for $0 < \frac{2r}{v_c} < 1$, as depicted in Fig. (3).

We now turn to a confined system with open boundaries at both ends. At this point we want to emphasize that there is a distinction between effects that arise from a non-trivial boundary condition (as discussed in Sec. IV A) and effects from a finite system size (which may or may not have trivial boundary conditions).

A confined system with open boundary conditions is technically more difficult to analyze, since the function $F(z)$ in Eq. (28) is periodic in z with twice the system size $2L$. Because of the non-integer exponents in Eq. (29), we need to carefully keep track of the overall phase as we integrate around the various branch-cuts. However, we can simplify things by explicitly using the short distance cutoff $z \rightarrow z - i$, which allows us to make a Taylor expansion of the factors in Eq. (29),

$$i \sin \frac{z}{2L} = \frac{e^{i\frac{z}{2L}} - X^{\frac{1}{2}}}{2} \sum_{n=0}^{\infty} c_n (i)^n e^{-in\frac{z}{L}} \quad (48)$$

with

$$c_n (i) = (i)^n \frac{(n+1)!}{(n+1)! (n+1)!} = \frac{(n+1)!}{(n+1)! (n+1)!}; \quad (49)$$

An immediate consequence of the periodicity is that $!$ gets discretized, which is consistent with the appearance of discrete energy levels for a finite system. The integral over the exponentials in the expansion (48) will give delta-functions at those special values of $!$ and we can try to extract an effective behavior in the prefactors, i.e. the coefficients c_n . For a single channel case we can verify by inspection that the asymptotic behavior of the prefactor in Eq. (49) gives the expected power-law for large n , i.e. the semi-infinite length result can be recovered.

However, for two channels and arbitrary values of $!$ we need to make a more careful analysis. By using the multiplication formula

$$\sum_{k=0}^{\infty} a_k X^k \sum_{k=0}^{\infty} b_k X^k = \sum_{k=0}^{\infty} c_k X^k \quad c_n = \sum_{k=0}^n a_k b_{n-k} \quad (50)$$

we derive from (29), (35), (38), and (48)

$$N(!; r) = \frac{1}{L} \frac{a_s + a_c}{2 \sin \frac{r}{L}} \sum_{n=0}^{\infty} \sum_{m=0}^{\infty} \frac{b_s + b_c}{2L} X^{\frac{r}{L}} \frac{X^{\frac{r}{L}}}{2L} f_n(a_c; b_c; r) f_m(a_s; b_s; r) \quad (51)$$

$$+ \frac{v_c(a_c + b_c)}{2L} \frac{v_s(a_s + b_s)}{2L} n \frac{v_c}{L} m \frac{v_s}{L} + \frac{v_c(a_c + b_c)}{2L} + \frac{v_s(a_s + b_s)}{2L} + n \frac{v_c}{L} + m \frac{v_s}{L};$$

where

$$f_n(k_1; k_2; r) = \sum_{p=0}^n c_n (k_1) c_p (k_2) \sum_{q=0}^{X^p} c_q (k_2=2) c_p (k_2=2) \cos(p - 2q) \frac{2r}{L}; \quad (52)$$

To understand the role of the delta-functions in (51) it is convenient to represent the argument of the delta function in a two-dimensional parameter space, coordinatized by the pair of summation indices $(n; m)$ in (51), as shown in Fig. (4). The line connecting $(!; 0)$ and $(0; !)$ indicates where the argument of the delta-function vanishes, and hence selects the terms to be included in the double sum in (51). The points are the allowed values of $!$ and the ratio $v_s = v_c$ determines the relative distances between the points in the x - and y -directions. This ratio plays a crucial role, because when $v_s = v_c$ is a rational number we have a resonance situation and the spectra will consist of peaks with constant spacing. On the other hand, for $v_s = v_c$ irrational, $N(!; r)$ is still discrete for small $!$ but approaches a continuous function for large $!$, since the number of points close to the line increases with increasing $!$. Moreover, if the spin-wave velocity v_s is significantly smaller than v_c the spectrum may appear continuous, but the discrete charge peaks may still be resolvable. (As $v_s \rightarrow 0$ the charge excitations are described by yet another exponent³⁴.)

When the (experimental) energy resolution $!$ is larger than the spacing between the peaks, it is appropriate to convert the infinite sums in Eq. (51) into integrations over continuous variables. The resulting double integrals can

actually be done exactly in the extreme boundary case as well as in the extreme bulk case, and the semi-infinite length results are recovered in both scenarios. Even for the intermediate case it appears that the coefficients (49) under the double sum closely reproduce the power-laws of the semi-infinite case if some smearing is taken into account. This is in strong contrast to the exponents that describe the momentum distribution, which are known to be strongly influenced by finite size effects as well as boundary effects¹⁸.

In conclusion, the main difference between a semi-infinite and a finite system is therefore the appearance of a discretized spectrum, with possible beatings of charge and spin excitations. This effect can only be observed in very small (mesoscopic) systems or with a very high experimental resolution, since the smeared spectral weight appears to follow the same frequency dependence. The effect of the boundary remains dominant for small frequencies in either case.

D. The finite temperature and finite length limit

The most general case is to consider both finite temperature and a connected system (finite length). The periodicity of the Green's function (25) is unchanged, but we expect that the coefficients in front of the delta-functions will acquire temperature dependent corrections similar to the ones discussed in Sec. IV B. We can make a similar Taylor-expansion as in the previous section by using Eq. (50) to expand the temperature dependent factor in Eq. (28) to the power of

$$\prod_{k=1}^{\infty} \left(1 + \frac{\sin \frac{z}{2L}}{\sinh k \frac{v}{2L}} \right)^{2k} = \prod_{k=1}^{\infty} \sum_{n=0}^{\infty} d_n(\beta; z) e^{kn \frac{v}{L}} \quad (53)$$

where

$$d_n(\beta; z) = \sum_{p=0}^{\infty} c_n^{(p)} \sum_{q=0}^{\infty} c_q^{(p)} \left(\frac{v}{L} \right)^{i(p-2q)\frac{z}{L}}; \quad (54)$$

and the coefficients c_n are defined in Eq. (49). This can be written as

$$\prod_{k=1}^{\infty} \left(1 + \frac{\sin \frac{z}{2L}}{\sinh k \frac{v}{2L}} \right)^{2k} = 1 + \sum_{m=1}^{\infty} \sum_{n=0}^{\infty} g_{n,m}(\beta) e^{in \frac{z}{L}} + e^{-in \frac{z}{L}} e^{-m \frac{v}{L}} \quad (55)$$

where $g_{n,m}(\beta)$ is a highly nontrivial but well-behaved function composed of the coefficients $c_n(\beta)$. The zero mode term H also makes a non-trivial contribution which will be discussed elsewhere³⁰.

The integration over the exponentials in Eq. (55) gives us again delta functions. However, there is no shift or smearing of the peaks in the spectra due to temperature, only the height of the existing peaks are modified, i.e. the points where the delta-functions contribute are at the same values of ω as indicated in Fig. (4). In the extreme boundary case we can derive an explicit (but complicated) expression for the spectral density and we observe that the temperature has a negligible effect for large ω as expected. We conjecture quadratic behavior of the coefficients for small ω , which is supported by preliminary numerical evidence, i.e. we observe a similar effect to the one discussed in section IV B. Thus, we are left with the analogous conclusion from the previous section that finite size effects always result in a discrete level spacing of delta-functions, but do not alter the (smeared) dependence on frequency. We therefore recover the same cross-over from ω^2 -behavior to boundary or bulk behavior as discussed in Sec. IV B.

V. DISCUSSION

In conclusion, we have derived an exact closed-form expression for the single-electron Green's function of a spinful Luttinger liquid at finite temperature and connected to a finite interval by open boundaries. By analyzing the corresponding spectral density we have obtained detailed information about the interplay between boundary, finite-size and temperature effects in an interacting electron system. Most importantly, we find that the scaling of the zero-temperature spectral density with frequency ω close to the Fermi level is always governed by a coupling-dependent boundary exponent significantly larger than the bulk exponent. In other words, the asymptotic low-energy behavior of a Luttinger liquid with an open boundary belongs to a different universality class than that of the bulk theory. Thermal fluctuations at finite temperature $T > 0$ destroy this behavior and open up a new regime for ω less than the temperature where the spectral density exhibits quadratic scaling in ω . Not surprisingly, the same effect is present in

a bulk system for this frequency range¹⁹, implying that the boundary plays no decisive role in the process. In the case of a finite interval confined by two open boundaries, our results reveal a discretized spectrum with delta-functions at the allowed energy levels. It is interesting to observe the dependence of spacing of the energy levels on the ratio $v_c=v_s$ between the effective velocities v_c and v_s of the charge- and spin excitations, respectively: For $v_c=v_s$ a rational number, the spectrum consists of well-separated peaks which, for sufficiently large l , coalesce to a quasi-continuum if $v_c=v_s$ is shifted to an irrational number. Although this effect can not be observed experimentally, it nonetheless suggests a resonance phenomenon with the collective charge and spin excitations showing interference effects at special values of the electron-electron coupling. However, despite the appearance of a discrete spectrum we find that finite size does not influence the l dependence of the integrated (i.e. smeared) spectral density significantly, so that the same boundary and finite temperature effects as for a semi-infinite can be observed.

Let us close by briefly discussing the possible relevance of our results to experiments, in particular the photoemission studies on the Bedgaard salts⁷ referred to in the introduction. These materials are composed of molecular chains which become conducting above some characteristic temperature T_c , and are expected to show Luttinger liquid behavior provided the temperature is high enough to mask the weak inter-chain coupling. However, as mentioned in the introduction, high-precision photoemission experiments indicate a scaling of spectral weight with frequency that is inconsistent with standard theory of a bulk Luttinger liquid: The effective exponent for scaling of the photoemission intensity is roughly 1.25 (Ref. 7) as also seen in independent NMR experiments on the same materials¹⁴, whereas the largest realistic value obtainable from a bulk Luttinger liquid description is $\nu = 0.125$, corresponding to the large-U Hubbard chain³. Attempts to include long-range Coulomb repulsion, which can be shown to increase²¹, fails due to the instability against an insulating phase at $\nu = 9=16^{35}$, so other explanations must be invoked. As the typical escape depth of photoelectrons in the UV range is only 5 - 10 Å, the experiments are extremely surface sensitive, suggesting that 1D boundary effects may play a role for the observed scaling behavior.

Consider first the case where one probes electrons that escape from a crystal face perpendicular to the 1D molecular chains. The photoemission intensity $I(l; \nu)$ is then proportional to the local spectral density $N(l; \nu; r)$, integrated over the escape depth of the photoelectrons, and weighted by the Fermi-Dirac distribution $f_{FD}(l; \nu)$

$$I(l; \nu) / \int_0^Z dr f_{FD}(l; \nu) N(l; \nu; r) : \quad (56)$$

In a boundary dominated region, $I(l; \nu)$ is seen to be dramatically reduced compared to the a bulk regime, considering our results in Eq. (43). With a typical escape depth of a few lattice spacings, the condition for boundary behavior $r = v_c < l$ may apply over an energy range of several hundred meV (since $v_c > aE_F$, with a the lattice spacing and with $E_F = 0.5 - 1$ eV, depending on the particular material²⁶).

In the recent photoemission experiments on $(\text{TM T SF})_2\text{PF}_6$ (Ref. 7), the chains are always in the plane of the cleaved surface³⁷, and it is less clear to what extent 1D boundary effects contribute. However, in the likely case that the cleaving of the surface introduces defects in neighboring chains, effectively breaking these into smaller segments, we may model the breaks by open boundaries and apply our results. Unfortunately, the actual defect concentration remains unknown, and it is therefore difficult to make a quantitative prediction from our results. This is an important issue that in principle should be possible to resolve via STM techniques. To explore the size of the boundary effects experimentally, it would also be of great interest to do photoemission experiments on cleaved surfaces that are perpendicular to the chains that could then be compared to the results from cleaved surfaces parallel to the chains.

As discussed in¹⁸, the finite-energy resolution of the photon lines effectively introduces an averaging over the "true" spectrum

$$I(l; \nu)_{\text{obs}} = \int_0^Z \frac{1}{2} e^{-(l-x)^2=2^{-2}} I(x) dx \quad (57)$$

which completely wipes out the power-law singularities in either the bulk- or boundary case. This "smearing" results in a similar effect as the thermal fluctuations, which also wipe out the sharp cusp from the power-laws as shown in Fig. (2), but have to be taken into account separately. With an experimental resolution of $\nu = 20$ meV and at a temperature $T = 50$ K (experimental values according to⁷), and assuming boundary dominated behavior for $N(l; \nu; r)$, the observed intensity in the vicinity of the Fermi level indeed appears to be depleted with an exponent of one or larger as shown in Fig. (5). (This should be compared to the large-U Hubbard exponent $\nu_{\text{bulk}} = 1=8$ of the bulk spectral function without temperature or averaging effects). In experiments the condition for boundary behavior $l < v_c=r$ will be satisfied over an energy range $l = E_F=r$ around the Fermi-level, where r is the distance from the boundary in units of the lattice spacing. This means that if the broken chains close to the cleaved surface have an average impurity density of a few percent, boundary effects could be observed over a region of up to 100 meV around the Fermi energy. Experiments indeed suggest a scaling $I(l; \nu)_{\text{obs}} / \nu^{\nu_{\text{obs}}}$ with $\nu_{\text{obs}} > 1$, extending, however, over a larger energy range. Thus, some additional mechanism (inter-chain coupling or electron-phonon coupling³⁸)

most likely have to be invoked to fully explain the data. Yet, a complete modeling of photoelectron spectroscopy on quasi-1D organic metals must certainly incorporate the boundary and temperature effects predicted in the present paper.

ACKNOWLEDGMENTS

We thank M. G. Rioni and J. K. Inaret for valuable correspondence. This work was supported in part by the Swedish Natural Science Research Council.

APPENDIX A: CALCULATION OF THE CHIRAL GREEN'S FUNCTION

Here we extend the calculations of Ref. 30 to the case of spinful Fermions with open boundaries. To calculate the chiral fermionic Green's function, we find it useful to treat the contributions from the zero modes and the dynamic bosonic modes separately. Hence we write $G_{\pm L}$ in Eq. (20) as a sum of the zero modes and the harmonic oscillator terms

$$G_{\pm L} = \frac{1}{2} (G_{\pm 0} + \tilde{G}_{\pm 0} + \hat{Q} \frac{x + vt}{2L} + S_{\pm L}) \quad (\text{A } 1)$$

where the bosonic operators are contained in the sum

$$S_{\pm L} = \sum_{n=1}^{\infty} \frac{1}{n} \frac{\hbar}{i} e^{i \frac{n(x+vt)}{L}} a_n + \text{h.c.} \quad (\text{A } 2)$$

We now insert this mode expansion into the bosonization formula (12) for $G_{\pm L}$, and use the definition of $G(x; y; t)$ $\frac{y}{L}; (x; t)_{\pm L}; (y; 0)$ to find

$$\begin{aligned} G(x; y; t) / H(x; y; t) &= \exp \frac{i}{4L} (vt + x - y) \\ &= c; s \\ &\exp \frac{\hbar}{2} (K + K^{-1})^2 B_{\pm L}(x; t; y; 0) \exp \frac{\hbar}{2} (K - K^{-1})^2 B_{\pm L}(x; t; y; 0) \\ &\exp \frac{\hbar}{4} (K^2 - K^{-2}) 2B_{\pm L}(x; t; y; 0) + 2B_{\pm L}(x; t; y; 0) \\ &B_{\pm L}(x; t; x; t) B_{\pm L}(x; t; x; t) B_{\pm L}(y; 0; y; 0) B_{\pm L}(y; 0; y; 0) \quad (\text{A } 3) \end{aligned}$$

Here we used the identity $e^A e^B = : e^{A+B} : e^{\frac{1}{2} [A, B]}$ for the bosonic operators $S_{\pm L}$ and we have defined the bosonic Green's function

$$B_{\pm L}(x; t; x^0; t^0) = S_{\pm L}(x; t) S_{\pm L}(x^0; t^0) - \frac{1}{2} [S_{\pm L}(x; t) S_{\pm L}(x; t) + S_{\pm L}(x^0; t^0) S_{\pm L}(x^0; t^0)] \quad (\text{A } 4)$$

The contribution from the zero modes is

$$H(x; y; t) = \sum_{c; s} \exp i u \frac{r}{2} \hat{Q} \quad (\text{A } 5)$$

where $u = \frac{1}{2L} v K^2 t + x - y$. This factor cannot be written as a product of spin and charge expectation values separately, because the quantum numbers n and m in Eq. (22) are connected by the condition that both are even or both are odd. However, since we know the quantization condition (22) and the energy spectrum (19) for the zero modes, we can directly sum over all eigenvalues $m; n$. The factor H can then be expressed in terms of the elliptic theta functions (see sections 8.18-8.19 in²⁸)

$$H(x; y; t) = \frac{\theta_2(u_c + c k_F L j_c) \theta_3(u_s j_s) + \theta_3(u_c + c k_F L j_c) \theta_2(u_s j_s)}{\theta_2(-c k_F L j_c) \theta_3(0 j_s) + \theta_3(-c k_F L j_c) \theta_2(0 j_s)} e^{i 2 u_c \frac{k_F L}{2}}; \quad (\text{A } 6)$$

where $\alpha = i \frac{v}{K 2L}$.

To calculate the bosonic Green's function B_{jL} , we insert the expression (A 2) for $S_{jL}(x;t)$ into Eq. (A 4), which gives

$$B_{jL} = \prod_{n=1}^{\infty} \frac{1}{4n} e^{2i \frac{v}{2L} \frac{v t + x - (v t^0 + x^0)}{2L}} (1 + m_n) + e^{2i \frac{v}{2L} \frac{v t + x - (v t^0 + x^0)}{2L}} (1 - m_n); \quad (A 7)$$

where m_n are the Bose-Einstein distributions

$$m_n = \frac{D}{a_n^y a_n^E} = \frac{1}{e^{\frac{n v}{L}} - 1}; \quad (A 8)$$

We define $a = e^{2i \frac{v}{2L} \frac{v t + x - (v t^0 + x^0)}{2L}}$ and $b = e^{\frac{v}{L}}$, which allows us to write

$$\frac{1}{1 - (b^{-1})^n} = \sum_{k=0}^{\infty} (b^{-n})^k = \sum_{k=0}^{\infty} (b^k)^n; \quad (A 9)$$

The bosonic Green's function can then be written as

$$\begin{aligned} B_{jL} &= \prod_{n=1}^{\infty} \frac{1}{4n} (a^n - 1) \sum_{k=0}^{\infty} b^{kn} + a^{-n} (1 - b^n) \sum_{k=0}^{\infty} b^{kn} \\ &= \prod_{k=0, n=1}^{\infty} \frac{1}{4n} a b^{kn} b^{kn} + a^{-1} b^{1kn} b^{1kn} \\ &= \prod_{n=1}^{\infty} \frac{1}{4n} (a^n - 1) + \prod_{k=1, n=1}^{\infty} \frac{1}{4n} a b^{kn} b^{kn} + a^{-1} b^{kn} b^{kn}; \end{aligned} \quad (A 10)$$

We now can use the formula

$$\sum_{k=1}^{\infty} \frac{z^k}{k} = -\ln(1-z); \quad |z| < 1 \quad (A 11)$$

and we need to use the high momentum cut-off in the first two terms of Eq. (A 10)

$$\prod_{n=1}^{\infty} \frac{1}{n} (a^n - 1) \approx \prod_{n=1}^{\infty} \frac{1}{n} (a^n - 1) c; \quad c = e^{-\frac{1}{L}}; \quad c \neq 0; \quad (A 12)$$

This yields

$$\begin{aligned} B_{jL} &= \frac{1}{4} \ln \frac{1}{c} \prod_{k=1}^{\infty} \frac{(1 - ab^k)(1 - a^{-1}b^k)}{(1 - b^k)(1 - b^k)} \\ &= \frac{1}{4} \ln 4 \frac{(ac)^{1=2}}{\frac{i}{2L}} \frac{(ac)^{1=2}}{2i} \frac{(ac)^{1=2}}{2i} \prod_{k=1}^{\infty} \left(1 + \frac{\frac{a^{-1=2}}{2i} \frac{a^{1=2}}{2i}}{\frac{b^{k=2}}{2} \frac{b^{k=2}}{2}} \right); \end{aligned} \quad (A 13)$$

Inserting a and b defined above gives us

$$B_{jL}(x;t; x^0; t^0) = \frac{i}{4} \frac{v t + x - v t^0 - x^0}{2L} \frac{1}{4} \ln F(v t + x - v t^0 - x^0) \quad (A 14)$$

where

$$F(z) = i \frac{2L}{2L} \sin \frac{z}{2L} \prod_{k=1}^{\infty} \left(1 + \frac{\sin \frac{z}{2L}}{\sinh k \frac{v}{2L}} \right) = \frac{\#_1 \left(\frac{z}{2L} \frac{v}{2L} \right)}{\#_1 \left(\frac{i}{2L} \frac{v}{2L} \right)}; \quad (A 15)$$

The first term in (A 14) cancels with the phase in the zero mode part of (A 3), resulting in Eq. (25).

Present address: Physics Department, Univ. of California at Santa Barbara, CA 93106.

- ¹ F. D. M. Haldane, *J. Phys. C: Solid State Phys.* 14, 2585 (1981).
- ² A. Luther and I. Peschel, *Phys. Rev. B* 9, 2911 (1974).
- ³ For a recent review, see J. Voit, *Rep. Prog. Phys.* 58, 977 (1995).
- ⁴ S. Tomonaga, *Prog. Theor. Phys.* 5, 544 (1950); J. M. Luttinger, *J. Math. Phys.* 4, 1154 (1963).
- ⁵ S. Tarucha, T. Honda, T. Saku, *Solid State Comm.* 94, 413 (1995).
- ⁶ A. Yacoby, H. L. Stormer, N. S. Wingreen, L. N. Pfeiffer, K. W. Baldwin, K. W. West, *Phys. Rev. Lett.* 77, 4612 (1996).
- ⁷ B. Dardel, D. M. Alterre, M. G. Rioni, P. W. Eibel, Y. Baer, and H. Levy, *Phys. Rev. Lett.* 67, 3144 (1991); Y. Hwu, P. A. Imbras, M. M. Arsi, H. Berger, F. Levy, M. G. Rioni, D. M. Alterre, and G. M. Margaritondo, *Phys. Rev. B* 46, 13624 (1992).
- ⁸ X. G. Wen, *Phys. Rev. B* 41, 12838 (1990); *Phys. Rev. B* 43, 11025 (1991).
- ⁹ P. W. Anderson, *Phys. Rev. Lett.* 64, 1839 (1990).
- ¹⁰ C. L. Kane and M. P. A. Fisher, *Phys. Rev. B* 46, 7268 (1992).
- ¹¹ K. Moon, H. Yi, C. L. Kane, S. M. Girvin, and M. P. A. Fisher, *Phys. Rev. Lett.* 71, 4381 (1993).
- ¹² F. P. Milliken, C. P. Umbach, R. A. Webb, *Sol. State Comm.* 97, 309 (1996).
- ¹³ For a review, see *Low-Dimensional Conductors and Superconductors*, ed. by D. Jerome and L. G. Caron (Plenum Press, New York, 1987).
- ¹⁴ P. W. Zietek, F. Creuzet, C. Bourbonnais, D. Jérôme, K. Bechgaard, P. Batail, *J. Phys. (Paris)* 3, 171 (1993).
- ¹⁵ K. Schonhammer and V. Meden, *Phys. Rev. B* 47, 16205 (1993) and (E) 48, 11521 (1993); J. Voit, *J. Phys. C: Cond. Mat.* 5, 8305 (1993).
- ¹⁶ Y. Suzumura, *Prog. Theor. Phys.* 63, 51 (1980).
- ¹⁷ G. Kirczenov, A. S. Sachrajda, Y. Feng, R. P. Taylor, L. Henning, J. Wang, P. Zawadzki, P. T. Coleridge, *Phys. Rev. Lett.* 72, 2069 (1994).
- ¹⁸ S. Eggert, H. Johannesson, and A. Mattsson, *Phys. Rev. Lett.* 76, 1505 (1996).
- ¹⁹ N. Nakamura, Y. Suzumura, *Prog. Theor. Phys.* 97, 163 (1997).
- ²⁰ J. Solyom, *Adv. Phys.* 28, 201 (1979).
- ²¹ H. J. Schulz, *Phys. Rev. Lett.* 64, 2831 (1990).
- ²² E. H. Lieb and F. Y. Wu, *Phys. Rev. Lett.* 20, 1445 (1968).
- ²³ For a collection of relevant papers, see M. Stone (ed.), *Bosonization*, (World Scientific, Singapore, 1994).
- ²⁴ J. M. Kosterlitz, *J. Phys. C: Solid State Phys.* 7, 1046 (1974).
- ²⁵ S. Mandelstam, *Phys. Rev. D* 11, 3026 (1975).
- ²⁶ E. Wong and I. A. Aeck, *Nucl. Phys. B* 417, 403 (1994).
- ²⁷ M. Fuentes, A. Lopez, E. Fradkin, *Phys. Rev. B* 53, 16568 (1996); A. Lopez, M. Fuentes, E. Fradkin, *Nucl. Phys. B*, in press.
- ²⁸ I. S. Gradshteyn and I. M. Ryzhik, *Table of Integrals, Series, and Products*, fifth edition, (Academic Press, San Diego, 1994).
- ²⁹ D. Loss, *Phys. Rev. Lett.* 69, 343 (1992); J. K. Inaret, M. Jonson, R. Shekhter, S. Eggert, *Phys. Rev. B*, in press.
- ³⁰ S. Eggert, A. Mattsson, J. K. Inaret, *Phys. Rev. B*, in press.
- ³¹ A. Kamelev and Y. Gefen, *Chaos, Solitons and Fractals* 8, 1229 (1997).
- ³² M. Fabrizio and A. G. Ogolin, *Phys. Rev. B* 51, 17827 (1995).
- ³³ See H. W. Diehl, in *Phase Transitions and Critical Phenomena*, Vol. 10, ed. by C. Domb and J. L. Lebowitz (Academic Press, London, 1986).
- ³⁴ K. Penc, F. Mila, H. Shiba, *Phys. Rev. Lett.* 75, 894, (1995).
- ³⁵ F. Mila and X. Zotos, *Europhys. Lett.* 24, 133 (1993).
- ³⁶ D. Jerome and H. J. Schulz, *Adv. in Physics* 31, 299 (1982).
- ³⁷ M. G. Rioni, private communication
- ³⁸ J. Voit and H. J. Schulz, *Phys. Rev. B* 37, 10068 (1988).

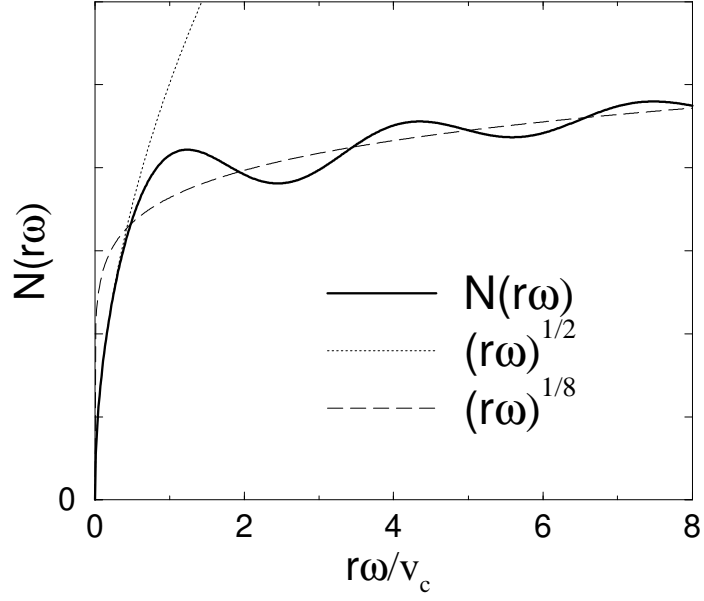


FIG .1. The spectral density as a function of $r\omega$ in arbitrary units (from Ref. 18). The corresponding power-laws for $\nu_{\text{bulk}} = 1/8$ and $\nu_{\text{bound}} = 1/2$ are also shown. The distance from the boundary r is held constant and just fixes the scale.

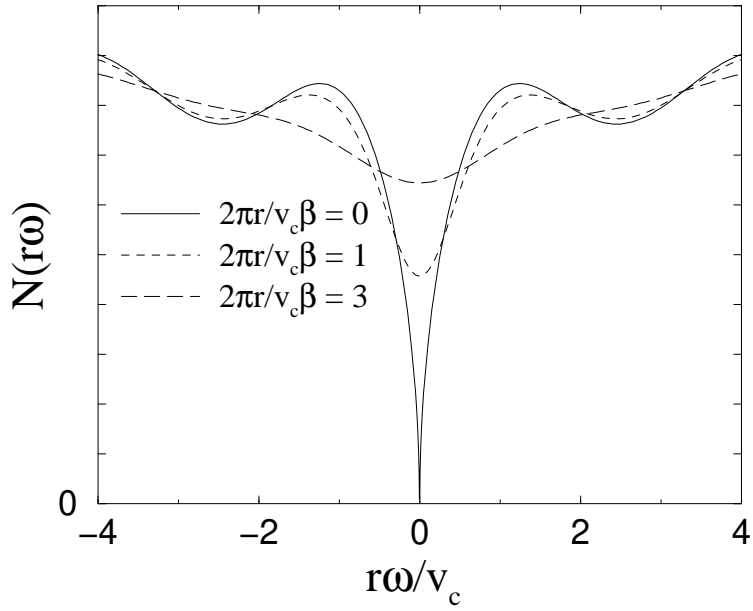


FIG .2. The spectral density as a function of $r\omega$ in arbitrary units for different temperatures $r = \dots$. For $\beta = 1$ we have parabolic behavior which crosses over to the $T = 0$ behavior for $\beta = \dots$.

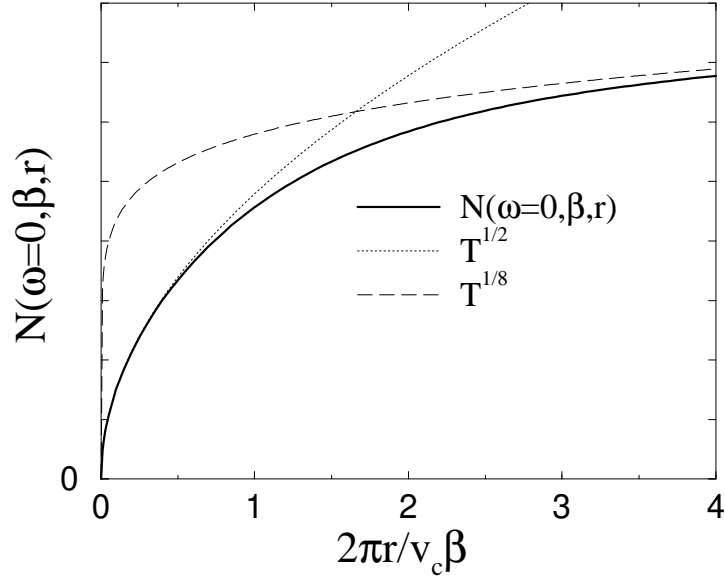


FIG .3. The spectral density at $\omega = 0$ as a function of $\frac{2\pi r}{v_c}$ in arbitrary units. The corresponding power-laws for $\nu_{\text{bulk}} = 1=8$ and $\nu_{\text{bound}} = 1=2$ are also shown. The distance r to the boundary is held fixed and sets the scales.

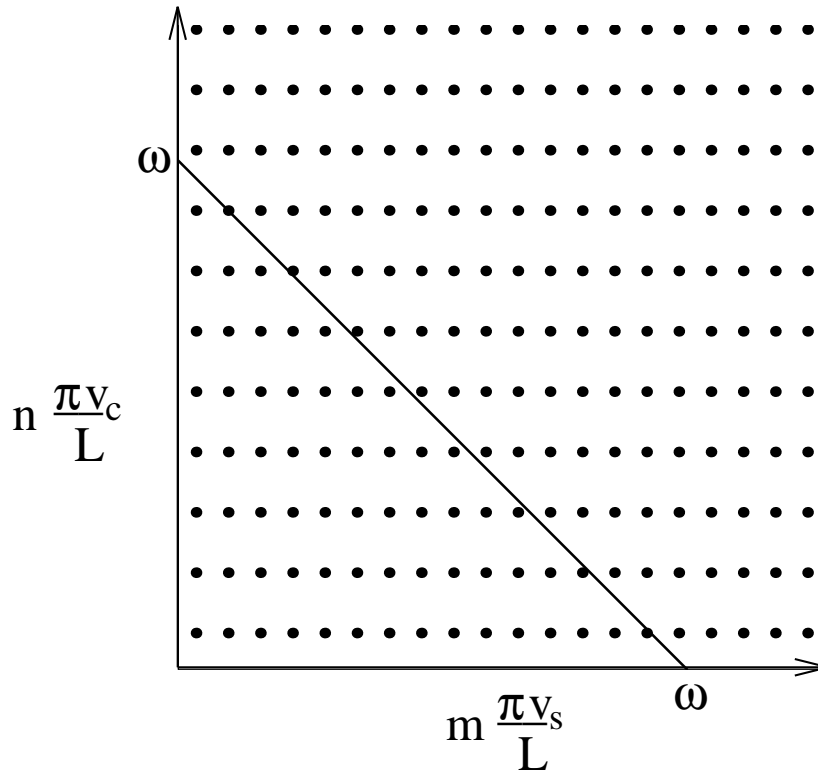


FIG .4. Illustration of the allowed values of ω (points) and the zeros of the argument of the delta-functions (line) in Eq. (51). The coordinates n and m are the summation indices. The line moves outward as ω increases and a delta-function appears in the spectral density at values of ω where the line crosses a point with coefficients as given in Eq. (51).

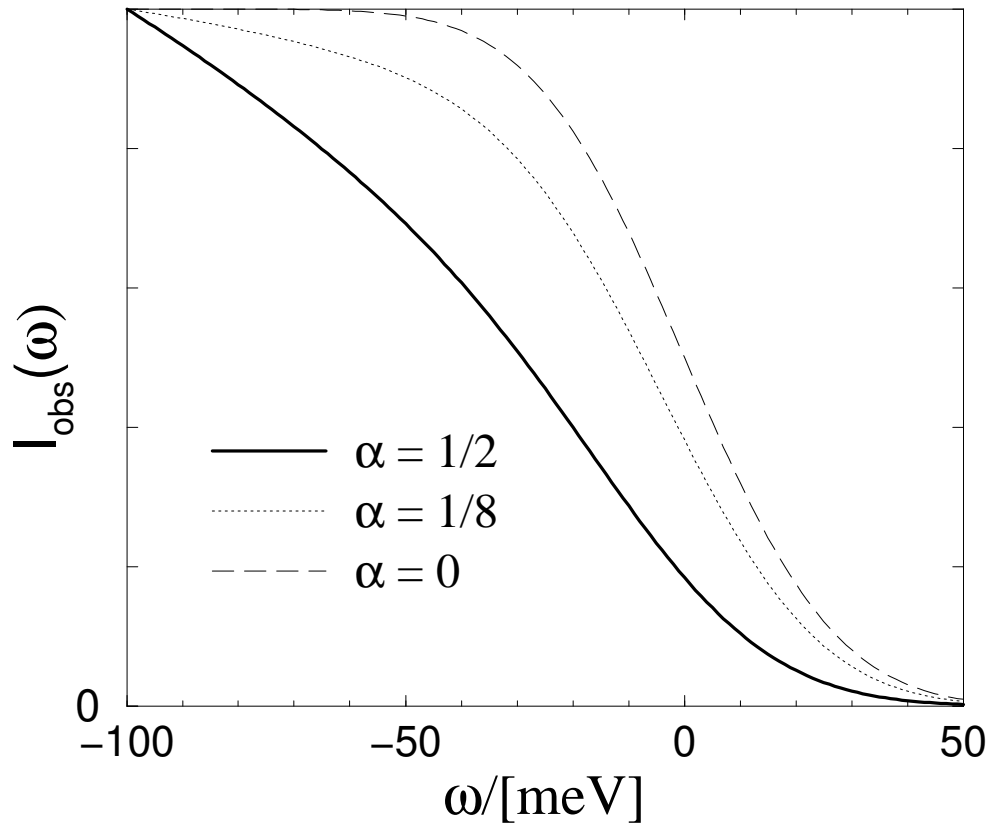


FIG. 5. The predicted intensity I_{obs} in arbitrary units as a function of ω for boundary and bulk cases (i.e. for power-laws with $\alpha_{\text{bound}} = 1/2$ and $\alpha_{\text{bulk}} = 1/8$, respectively). The corresponding three-dimensional case ($\alpha = 0$) is also shown. Temperature ($T = 50\text{K}$) and finite resolution ($\Delta = 20\text{meV}$) effects have been taken into account.